Journal Pre-proof

Facile green synthesis of magnesium oxide nanoparticles using tea (*Camellia sinensis*) extract for efficient photocatalytic degradation of methylene blue dye

S. Ashok Kumar, M. Jarvin, S.S.R. Inbanathan, Ahmad Umar, N.P. Lalla, Nelson Y. Dzade, Hassan Algadi, Qazi Inamur Rahman, Sotirios Baskoutas

Please cite this article as: S.A. Kumar, M. Jarvin, S.S.R. Inbanathan et al., Facile green synthesis of magnesium oxide nanoparticles using tea (*Camellia sinensis*) extract for efficient photocatalytic degradation of methylene blue dye. *Environmental Technology & Innovation* (2022), doi: https://doi.org/10.1016/j.eti.2022.102746.

This is a PDF file of an article that has undergone enhancements after acceptance, such as the addition of a cover page and metadata, and formatting for readability, but it is not yet the definitive version of record. This version will undergo additional copyediting, typesetting and review before it is published in its final form, but we are providing this version to give early visibility of the article. Please note that, during the production process, errors may be discovered which could affect the content, and all legal disclaimers that apply to the journal pertain.

Facile Green Synthesis of Magnesium Oxide Nanoparticles using Tea (*Camellia Sinensis*) Extract for Efficient Photocatalytic Degradation of Methylene Blue Dye

S. Ashok Kumar[1], M. Jarvin[1], S. S. R. Inbanathan[1]*, Ahmad Umar,[2,3] N. P. Lalla[4], Nelson Y. Dzade,[5,6]Hassan Algadi,[2,7]Qazi Inamur Rahman,[8]Sotirios Baskoutas[9]

[1] *Post Graduate & Research Department of Physics, The American College, Madurai -625002, Tamilnadu India*

[2] *Department of Chemistry, Faculty of Science and Arts, Najran University, Najran-11001, Kingdom of Saudi Arabia.*

[3] *Promising Centre for Sensors and Electronic Devices (PCSED), Najran University, Najran, 11001, Kingdom of Saudi Arabia.*

[4] *UGC-DAE Consortium for Scientific Research, Indore-452001 India*

[5] *Cardiff University, Main Building, Park Place, CF10 3AT, Cardiff, United Kingdom*

[6] *Department of Energy and Mineral Engineering, Pennsylvania State University, University Park, PA 16802, United States*

[7] *Department of Electrical Engineering, Faculty of Engineering, Najran University, P.O. Box 1988, Najran 11001, Kingdom of Saudi Arabia.*

[8] *Department of Chemistry, Integral University, Lucknow-226026, India*

[9] *Department of Materials Science, University of Patras, 26504, Rio, Patras, Greece*

Corresponding author:*ssrinbanathan@gmail.com (S. S. R. Inbanathan**)

Abstract

Herein, we report, for the first time, the synthesis, characterization, and the photocatalytic methyl blue dye degradation performance of magnesium oxide (MgO) nanoparticles (NPs) synthesized by a facile green approach using *Camellia sinensis* (tea leaves) extract as a reducing agent. The as-prepared materials were characterized by x-ray diffraction (XRD), which confirmed the large-scale synthesis of well crystalline cubic crystalline phase MgO NPs. Rietveld refinement analysis of the XRD pattern was done to determine the crystallographic parameters of the MgO NPs and to investigate lattice defects. Microstrain, lattice stress and energy density were calculated using Williamson-Hall analysis. The synthesized nanoparticles exhibited over 97% photocatalytic degradation efficiency of methylene blue (MB) dye. Complementary density functional theory (DFT) calculations revealed the favorable formation of O_2^- radicals on the MgO (001) surface as the drivers of the MB dye degradation.

Key words: *Camellia sinensis*, MgO nanoparticles, MB dye, photocatalysis.

1.   Introduction

Water contamination by organic dye discharges from textile dyeing, paper making, paints, cosmetics, and food processing industries has attracted considerable attention recently owing to health hazards posed to humans and of other living organisms [1-3]. Due to their color and toxic products generated through hydrolysis and oxidation reactions in the wastewater phase, the discharge of effluents containing low-biodegradable dyes into the water bodies is not desirable [4-7]. Among the various methods for treating dye-contaminated water, photocatalytic degradation of organic pollutants has received significant attention [8-10]. The traditional technologies for treating wastewater in particular coagulation, adsorption,

flocculation, advanced oxidation, and precipitation do not only require long operation times, but they also produce secondary sludge, which is expensive to dispose [11, 12].

Inorganic materials such as metal and metal oxides in nano-dimensions have received considerable attention in recent years owing to their potential use in several applications, including photocatalytic dye degradation [13-15]. Several transition metal oxide photocatalysts, such as MO (M=Ni, Zn, Mg, and Cu) and TiO_2 have been investigated for their performance in dye degradation [16-20]. Among these, magnesium oxide (MgO) is attractive for photocatalytic applications owing to its non-toxicity, earth-abundance and ideal physicochemical and optoelectronic properties [21-24]. MgO nanoparticles have been used in several technological applications, such as electronics, catalysis, ceramics, petrochemical products, coatings, and pharmaceuticals [25, 26]. Highly crystalline MgO NPs are characterized by low electrical conductivity, higher melting point, large surface areas and unusual crystal morphologies [27].

Several methods have been explored to synthesize MgO nanoparticles including the hydrothermal, sol-gel, co-precipitation, and chemical gas phase methods [21-28]. However, in general these methods use several toxic reagents, strong acids and bases to synthesize MgO, which create environmental problems. Hence, it remains a challenge to synthesize MgO nanoparticles using safe, eco-friendly, and low-cost approaches. Recent efforts have turned towards the development of green synthesis approaches, where organisms such as yeast, bacteria, sugars, algae and polymers and plant extracts are used for the synthesis of nanoparticles [29-31].

Herein, we demonstrate a facile synthesis of MgO nanoparticles using *Camellia sinensis* (tea leaves) extract as a reducing agent [21, 27, 32].Tea leaves extract contains polyphenols and that helps in reduction of salt precursor to nanoparticles. Flavonoids and catechin present in the polyphenols. Epigallocatechin Gallate(EGCG) is the dominant catechin take part in the reduction of salt precursors and responsible for formation of MgO

nanoparticles (see the experimental details in the ESI†) [27,42].This method is simple and does not require any toxic chemicals and sophisticated instrumentation. Fig. S1 represents the schematic diagram of how the MgO nanoparticles were prepared (see the ESI†). The prepared MgO NPs were systematically characterized using a range of characterization techniques to determine the structural, morphological and optical properties. From XRD, the crystallite size was calculated using Scherrer's formula. Microstrain, lattice stress and energy density of thus prepared MgO NPs were calculated using Williamson-Hall (W-H) analysis or X-ray peak profile analysis (XPPA) [43-50]. The Willianson-Hall technique is a well-known method for analysing X-ray pattern peak broadening induced by crystallite size reduction and internal micro-strain. Instrumental effects, crystallite size reduction, and micro-strain in the crystal lattice all contribute to the widening of X-ray diffraction patterns. Crystallite size and lattice strain both impact Bragg peak in different ways, causing the peak breadth and intensity. As a photocatalyst, the as-prepared MgO NPs show efficient photocatalytic degradation (~97%) of methylene blue dye.

2. Photocatalytic activity of MgO nanoparticles

The catalytic activity of the as-preparedMgO NPs was investigated by choosing a model azo dye methylene blue (MB) under UV illumination at ambient temperature. The photocatalytic experiments were carried out in a slurry type batch reactor [33]. The UV visible spectra of the MB dye show a strong absorption peak at 665 nm [34]. For the photocatalytic application, a stock solution (1 mg/L) was prepared by stirring it in the dark. An appropriate amount of (0.025g) MgO photocatalyst was taken for 100 ml of the dye solution. Afterwards the resultant MB dye and MgO nano-powder suspension was kept under dark and stirred for 30 min to get absorption or desorption equilibrium. Then the solution was irradiated under UV-light from a photo-reactor (8W), which is fitted with a magnetic stirrer encircled by a water circulation arrangement to maintain temperature. After a specific time interval of 30 min, 10 ml aliquots dye solution was analyzed by UV-visible

spectrophotometer to study the absorption behavior of decomposed dye solution. Generally, the photodegradation of MB dye followed the pseudo-first order kinetics and degree of degradation was expressed by (C/Co) with respect to time, C/Co is the ratio of MB concentration at a time to the initial concentration. The percent degradation was calculated using equation 1 below [9]:

$$\%Degradation = \frac{C_o - C}{C_0} \times 100 \qquad (1)$$

where C_o = initial MB dye concentration, and C = concentration of the MB dye solution after the degradation time 't'.

2.1 Computational details

The dispersion-corrected density functional theory (DFT-D3) calculations were carried out within the VASP-Vienna Ab initio Simulation Package [35, 37].Description of the interactions between the core and valence electrons was done using the Project Augmented Wave (PAW) method [36]. The kinetic energy cutoff was set to 600 eV and a Monkhorst-Pack k-point mesh of 9×9×9 was used to sample the Brillouin zone of bulk MgO. The conjugate-gradient algorithm was employed for geometry optimization, ensuring that residual forces on all atoms reached 10^{-3} eV/Å. The Exchange-correlation functional was described using the Perdew–Burke–Ernzerhof (PBE) scheme of generalized gradient approximation [38]. The lattice parameter of MgO modelled in the rock salt structure is calculated at a = 4.237 Å, which is in good agreement with the experimental value of 4.216 Å. The DFT+U method with an effective U value of 4 for Mg was used to predict electronic structure and band gap. The adsorption mechanism of O_2molecule was characterised on the MgO(001) surface, which was created using the METADISE code [39]. Charge transfer between the MgO(001) surface and the absorbing molecules was quantified using Bader charge analysis [40].

2.2 Statistical Analysis:

Experiments were carried out in triplicates for the dye degradation experiments and the results are expressed as the attributes of best fit using origin software. The degradation efficiency is statistically significant at $\alpha_{0.05}$ and $\alpha_{0.01}$ and was found to be 0.13959 with 9 degrees of freedom. For X-ray line profile analysis origin software were used which has in built standard error statistical tools.

3. Results and discussion

3.1. Characterization of structural properties of as-prepared MgO nanoparticles

3.1.1 XRD analysis

The XRD pattern of as-prepared sample (Fig. S2(a) see the ESI†) exhibited several peaks which correspond to unreacted precursors, *i.e.* magnesium nitrate hydrate (nitromagnesite). The peaks disappeared after calcination of the sample at 400 °C. The calcined sample displays well-defined peaks at $2\theta = 37.07°$, $43.03°$, $62.39°$, $74.76°$, and $78.68°$, which can be assigned to (111), (200), (220), (311), and (222) planes of MgO respectively [41, 42]. The observed results are consistent with the standard JCPDS Card no: 77– 2364.

The lattice parameters of MgO NPs were determined from Rietveld refinement analysis using the FULLPROOF software [51]. The space group for the MgO NPs was assumed to be Fm-3m (225) for the cubic crystal system. The lattice parameter, atomic coordinates and the Wyckoff notations are given in Table S1 (refer ESI†). The refinement (fitting) parameters (R_p, R_{wp} and R_{exp}) are consistent with the refined standard pattern of MgO nanoparticles for the cubic structure [51-55], which is shown in Fig. S2(b). The packing diagram for the cubic MgO structure is shown in the inset of Fig. S2(b) (refer ESI†).

3.12 Scherrer method

The average crystallite size of the as-prepared MgO NPs was calculated using Debye-Scherrer's equation as given below [7]:

$$D = \frac{K\lambda}{\beta \cos\theta} \quad (2)$$

Where D is the crystal size, k is the shape factor (usually taken as 0.9), λ is the wavelength of the Cu-Kα radiation (λ= 0.15406nm), β is the Full width half maximum (FWHM) and θ is the angle of reflection. The FWHM for the reflections were obtained after applying correction for the instrumental broadening using the method of Anantharaman and Christian [56]. According to the above equation, the average crystallite size of the synthesized MgO NPs was found to be 35±4 nm.

3.1.3 Williamson-Hall analysis

X-ray analysis is an excellent non-destructive tool for fine structure investigation of matter not only for crystal structure determination but also for studying various physical properties of materials. Especially, Williamson- Hall (W- H) analysis, which is employed in this work, is a simplified integral breadth method and is used to deconvolute the size and lattice strain induced line broadening. The Scherrer equation deals only on the effect of crystallite size in XRD line broadening and it cannot be considered for microstructures of the lattice, i.e., about the intrinsic strain, which are due to the point defects, grain boundaries, triple junctions, and stacking faults[43,49]. Williamson–Hall (W-H) is one of the methods where the strain-induced XRD peak broadening is considered. This method provides an estimation of of the crystal size along with the intrinsic strain from defects like distortion, twinning, imperfection, and dislocation [50].

Uniform Deformation Model (UDM)

In this model it is assumed that the strain in the crystal is uniform in the whole crystalline-geometric directions, implying that the crystal is isotropic in nature. The lattice strain and distortion was calculated by the following equation

$$\varepsilon = \frac{\beta_{hkl}}{4\tan\theta} \tag{3}$$

It follows that

$$\beta_{hkl} = \left(\frac{k\lambda}{D\cos\theta}\right) + 4\varepsilon\sin\theta \tag{4}$$

By rearranging the equation, we get

$$\beta\cos\theta = \frac{K\lambda}{D} + 4\varepsilon\sin\theta \tag{5}$$

Equation (5) represents W-H equation for Uniform Deformation Model (UDM). From the plot of $4\sin\theta$ (x-axis) vs. $\beta\cos\theta$ (y-axis) one can obtain the strain ε and crystallite size D. Fig. S3 (a) (see ESI†) shows Y-intercept gives the value of crystallite size and slope represents the strain. This strain might be related to lattice shrinkage.

Uniform Stress Deformation Model (USDM)

In this model Hooke's law is employed with the assumption that the NPs having small strain. Therefore the W–H equation of UDM can be altered by applying Hooke's law $\sigma = Y\varepsilon$, σ represents stress and *Y* denotes the Young's modulus of elasticity. Equation (5) can be rearranged by applying Hooke's law as follows

$$\beta\cos\theta = \frac{K\lambda}{D} + \frac{4\sigma\sin\theta}{Y_{hkl}} \tag{6}$$

The above equation (6) is called the Uniform Stress Deformation Model (USDM).

$$\frac{1}{Y_{hkl}} = S_{11} + 2(S_{11} - S_{12} - 0.5S_{44})(m_1^2 m_2^2 + m_2^2 m_3^2 + m_3^2 m_1^2)$$ (7) [49]

Here, the 'Y_{hkl}' is Young's modulus. Where S_{ij} are the elastic compliance (for cubic MgO S_{11} = 4.01, S_{12} = -0.96 and S_{44} = 6.46 (TPa)$^{-1}$), whereas m_1 = h (h^2+k^2+l^2), m_2 = k (h^2+k^2+l^2) and m_3 = l (h^2+k^2+l^2). By using the above equation (7), the Y_{hkl} value of MgO NPs was found to be 212±1 GPa. From the plot of 4sinθ/Y (x-axis) vs. βcosθ (y-axis) one can obtain the stress σ and crystallite size D. The crystallite size was obtained from Y-intercept and the lattice stress from the slope (refer Fig. S3 (b)) (see ESI†).

Uniform Deformation Energy Density Model (UDEDM)

The anisotropic energy can be studied by this Uniform Deformation Energy Density Model (UDEDM). In this model it is assumed that the lattice energy density is associated with effective stiffness of a crystal. Based on this assumption energy density 'u_{ed}' is written as follows

$$u_{ed} = \frac{(\varepsilon^2 Y_{hkl})}{2}$$ (8)

Then the equation (4) can be simplified as the energy and strain relation

$$\beta\cos\theta = \left(\frac{k\lambda}{D}\right) + \left(4\sin\theta\left(\frac{2u}{Y_{hkl}}\right)^{1/2}\right)$$ (9)

From the plot of 4sinθ(2/Y)$^{0.5}$ (x-axis) vs. βcosθ (y-axis) one can get energy density u and crystallite size D. From the Fig. S3 (c) (see ESI†), the crystallite size was calculated from Y-intercept and the energy density value from the slope.

It is evident from the Table S2(see the ESI†), crystallite size obtained from the three models of W-H is almost similar to the value obtained from Scherrer method with an standard error

of $\pm$ 4 nm. In addition, the values of strain and stress are found to be compressive, i.e. positive values in all (hkl) crystallographic parameters (refer Table S2†). The difference in the strain value obtained from UDM-USDM with the UDEDM may due to the uniformity of the deformation [50]. The small difference in the crystallite size values obtained from Scherrer's equation and W-H analysis may be due to the averaging of the particle size distribution.

*3.1.3 Morphological, compositional, optical and thermal propertie*s

The general morphology of the as-prepared MgO NPs was studied by scanning electron microscopy (SEM). As observed in the SEM micrograph, the general morphology of the as-prepared MgO material was examined by and the result is demonstrated in Fig. 1(a). As observed in the SEM micrograph, the as-prepared MgO material possesses nano-scale particle shaped morphology, thus one can refer to it as 'nanoparticles'. Owing to dense growth, some agglomeration in the nanoparticles is also observed. The MgO nanoparticles exhibit spherical-shape with smooth surfaces. The average particle size of the MgO NPs was determined from four micrographs, taken from different areas, of the sample using Image J software and the size of NPs are found to be in the range of 65 $\pm$ 5 nm.

The chemical composition and purity of the as-prepared MgO NPs was examined by Fourier transform infrared (FTIR) spectroscopy as shown in Fig. 1(b). The response of the FTIR spectrum was observed in the range of 4000$-$ 450 cm^{-1}. The board peak within the range of 3600 cm^{-1} to 3200 cm^{-1} can be attributed to the presence of OH groups [5-7]. Due to the presence of water molecules, O-H vibrations are assigned at 3435 cm^{-1} [6]. The peak at 2929 cm^{-1} can be assigned to the asymmetric –CH$_2$ vibration [12]. This peak could also indicate the adsorption band [27]. The peaks at 1583 and 1435 cm^{-1} correspond to the C=C stretching and C-N stretching, respectively [6-8]. The peak at 1108 cm^{-1} is related to the C-O stretching vibrations. The appearance of these peaks at 2929 and 1108 also proves the

presence of polyphenols, carboxylic acid, polysaccharide, amino acid, and proteins in tea extract [27]. The peak at 496 cm^{-1} confirms the presence of M-O (MgO) peak [8, 9].

From UV-visible spectroscopy analyses, the optical properties of the prepared MgO nanoparticles were determined. Fig. 1(c) depicts the typical plot for $(\alpha h v)^2$ vs energy used to estimate the band gap of the prepared MgO nanoparticles at ~4.21 eV.
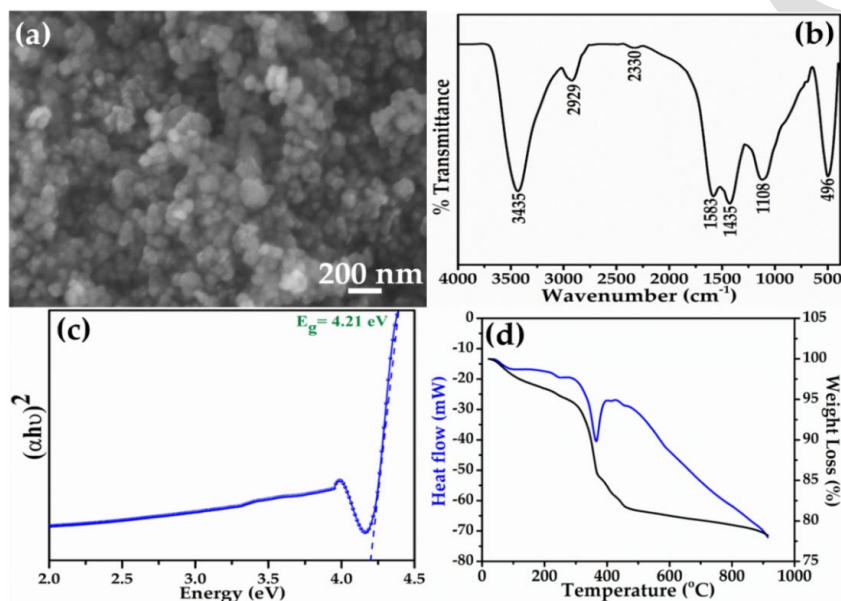

Fig. 1. Typical (a) SEM , (b) FTIR spectrum, (c) Energy band gap (Tauc plot), and (d) TGA-DSC for the prepared MgO nanoparticles.

To examine the thermal properties of the prepared MgO nanoparticles, thermogravimetric analysis (TGA) and differential scanning calorimeter (DSC) analysis were done and results are shown in Fig. 1(d). The observed thermogravimetric analysis (TGA) curve shows the amount of weight loss during the calcination process. The prepared MgO nanoparticles exhibit weight loss in two steps, i.e. the first one from 43.39 ^{o}C to 157.27 ^{o}C, which corresponds to 99 % to 96 % of dehydration, *i.e.* removal of water. The second step occurred from 309.84 ^{o}C to 475.24 ^{o}C and corresponds to the decomposition process of organic moieties to form MgO. Interestingly, the differential scanning calorimeter (DSC) shows a strong endothermic peak at the 365.32 ^{o}C [57-59].

3.2. Photocatalytic activity of MgO nanoparticles

The photocatalytic activities of the as-prepared MgO NPs were successfully demonstrated over MB dye. Fig. 2(a) shows the characteristic UV-Vis absorption spectra of MB dye aqueous solution in the presence of the as-prepared MgO nanoparticles irradiated by UV light for different time intervals (0-120 min). It is interesting to note that there is a gradual decrease of absorption intensities at λ_{max} 664 nm which confirmed the MB dye discoloration reaction. Fig. 2(b) depicts the extent of MB dye discoloration with successive time intervals in the absence and presence of the as prepared MgO NPs. Interestingly, a negligible degradation of MB took place under the UV light, suggesting that UV light alone cannot degrade the MB dye. However, there was almost a complete degradation (97 %) of MB dye in the presence of the as-prepared MgO NPs.

Usually, the kinetics of MB dye degradation followed the Langmuir–Hinshelwood model and the rate constant can be calculated using the following equation [60]
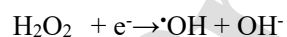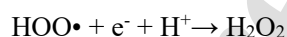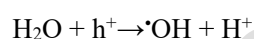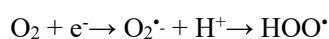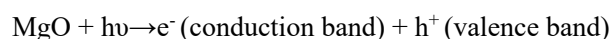
$$r = -\frac{dC}{dt} = \frac{kKC}{1+KC} \quad (10)$$

where, r is rate of dye discoloration (mg/1 min), C represents the concentration of dye (mg/l), t defines the time of illumination, K is the adsorption coefficient of dye (l/mg), and k is the rate constant (mg/l min). For a very dilute solution, C would be very small, hence, the equation 10 could be written as:
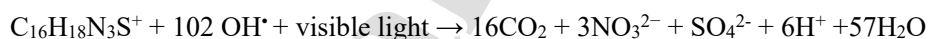
$$\ln\frac{C_0}{C} = kKt \approx k_{app}t \quad (11)$$

where K_{app} is the apparent rate constant. Fig. 2(c) represents the typical first order kinetics graph of MB dye photodegradation reaction. A plot of ln (C$_o$/C) *vs* time gives a straight line with the slope equal to the first-order rate constant. The calculated apparent rate constant k$_{app}$ and regression coefficient R^2 for the as-prepared MgO nanoparticles were 0.0293 min^{-1} and 0.9857, respectively. The observed results are consistent with the reported literature [61, 62].

Fig. 2(d) depicts the mechanism of MB dye discoloration reaction. The illumination of the as-prepared MgO with photons of appropriate wavelength leads to electron-hole (e^-/h^+) pairs generation [63]. When the UV light strikes on the photocatalyst, electrons (e^-) would be excited from the valence band to the conduction band to react with the surface of the photocatalyst to produce superoxide ions (O_2^-), which subsequently upon protonation produced $HOO^•$ radicals. Further reaction of the $HOO^•$ radicals with e^- yields H_2O_2. Simultaneously, the holes (h^+) in the valence band react with water to produce H_2O/ OH-radicals in the oxidation process. Overall, the reaction can be summarized as follows:

$MgO + h\upsilon \rightarrow e^-$ (conduction band) $+ h^+$ (valence band)

$$O_2 + e^- \rightarrow O_2^{•-} + H^+ \rightarrow HOO^•$$

$$H_2O + h^+ \rightarrow {}^•OH + H^+$$

$$HOO^• + e^- + H^+ \rightarrow H_2O_2$$

$$H_2O_2 + e^- \rightarrow {}^•OH + OH^-$$

It has been successfully reported that the degradation of MB dye starts via splitting of the $C-S^+$, $=C$ bond and afterwards leads to complete conversion of nitrogen, carbon and sulfur hetero atoms into NH_4^+, NO_3^{2-}, CO_3^{2-} and SO_4^{2-} mineralization ions as summarized [53];

$$C_{16}H_{18}N_3S^+ + 102\ OH^• + \text{visible light} \rightarrow 16CO_2 + 3NO_3^{2-} + SO_4^{2-} + 6H^+ + 57H_2O$$

Formation of highly active oxygen radicals $\{O_2, O_2^{•-}, OH^- \text{ or } HOO^•\}$ were responsible for facile degradation of MB dye. The failure of photogenerated e^-/h^+ pairs to reach their respective sites leads to their recombination, which is often the primary origin of reduced photodegradation efficiency. Since the photocatalytic reaction was facilitated over the surface of as-prepared MgO nanoparticles, the structural and morphological properties would have an impact on the photocatalytic efficiency. The uniform and high crystalline MgO nanoparticles could minimize the rate of recombination of photogenerated e^-/h^+ pairs and lead to efficient photodegradation [64]. The observed efficient degradation of MB dye reveals that the MgO

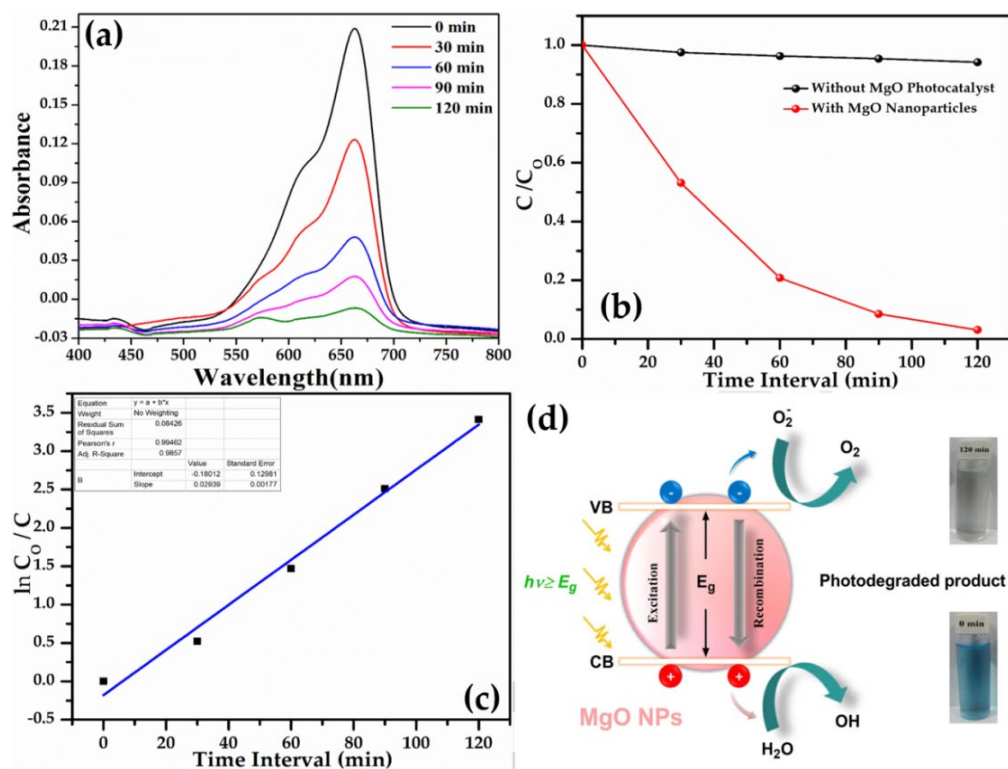nanoparticles can serve as efficient photocatalysts to degrade organic dyes under UV light illumination.

Fig. 2 (a) UV–Vis absorbance spectra of decomposed methylene blue dye solution, (b) the curve of C/Co versus time interval over MgO nanoparticles, and (c) first order kinetics graph of MB dye photodegradation reaction, and (d) Schematic mechanism for the photocatalytic degradation of MB dye using MgO nanoparticles.

The reusability of MgO NPs as a photocatalyst in MB dye decomposition process, have also been tested. The NPs were centrifuged and washed, three times, thoroughly before using for each cycle. The photodegradation experiments were repeated three times, under similar conditions, and the corresponding degradation results show 97%, 86%, and 77% of dye degradation for the first, second and third cycle,respectively. This results shows that the NPs have good reusability and photo-stability.

3.3 DFT calculations

Further molecular-level insights into the formation of O_2^- radicals and OH^- species on the MgO surface, which are expected to facilitate the degradation of the MB dye, was gained through first-principles DFT calculations [65]. The structural and electronic properties of the bulk MgO was first determined, predicting a bandgap of 4.52 eV as shown in Fig. S4 (a) (see the ESI†). Fig. S4 (b) (see the ESI†) the Mg(001) surface was used to characterize the adsorption reactions of O_2 and H_2O molecules.. The valence and conduction band edges are shown to be dominated by O-p states. Fig. 3 (a-d) shows the lowest-energy O_2 adsorption structures on the MgO(001) surface. The end-on adsorption geometry of O_2 released an adsorption energy of −0.86 eV, whereas a side-on geometry released an adsorption energy of −1.14 eV. These results show that the side-on O_2 geometry is energetically more stable than the end-on configuration. The O−O bond distance for the side-on and end-on adsorption configurations is respectively calculated at 1.251 Å and 1.248 Å. This indicates a small elongation in the adsorbed O−O bond distance relative to the gas phase O_2 molecule (1.240 Å). The O_2 molecule gained 0.48 and 0.28 e^- from the surface when adsorbed in the side-on and end-on configurations, respectively, as estimated from Bader charge analysis. This characterizes the adsorbed species as O_2^- radicals.

The adsorption of water and its subsequent dissociation to form OH^- species has also been investigated as shown in Fig. 3 (e-g). Whereas the adsorption of molecular water is exothermic by −0.47 eV, the dissociative adsorption is endothermic by +0.43 eV and +0.68 eV when the proton is adsorbed at O or Mg sites, respectively. The endothermic reaction of the dissociative species suggests that OH^- species formation will be thermodynamically limited on the MgO(001) surface. This therefore, suggests the O_2^- radicals, which are thermodynamically favorable, are the main facilitators of MB dye degradation.
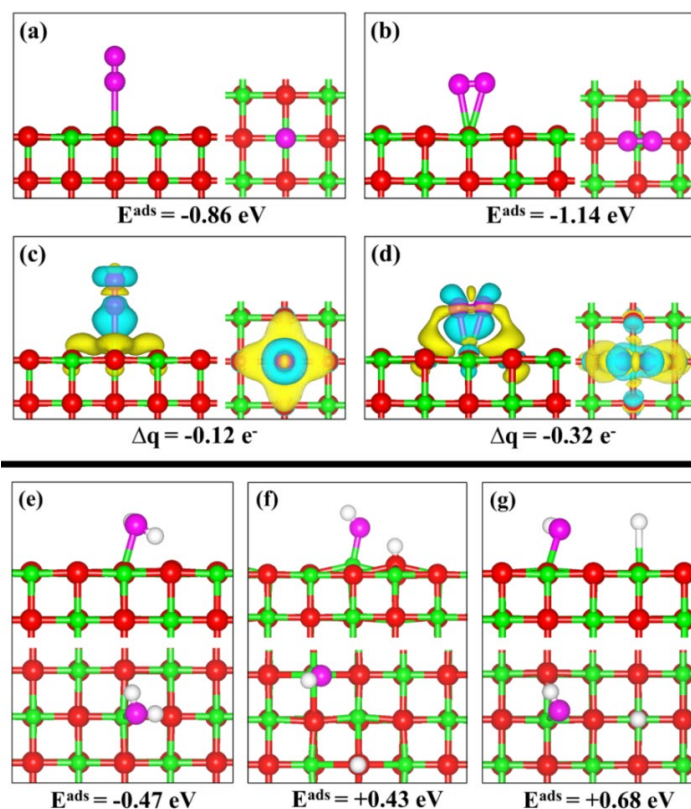
Fig. 3. The optimized adsorption geometries of O_2 in (a) end-on and (b) side-on configurations at MgO(001) surface. The corresponding charge density difference iso-surface contours (c & d), with the green and yellow contours indicating electron density increase and decrease by 0.003 e/$Å^3$, respectively. The molecular (e) and dissociative adsorption ((f) & (g)) of water. Atomic color: Mg =green, O_{surf} =red, O_{mol} = pink, and H =red.

4. Conclusion

In summary, MgO NPs were synthesized by facile green approach using *Camellia sinensis* (tea leaves) extract as a reducing agent. The morphological, structural, optical, thermal and photocatalytic properties of the as-prepared MgO nanoparticles were systematically characterized. Rietveld refinement analysis of XRD patterns shows cubic crystal structure and indicates the presence of Mg and O vacancies. The average crystallite size was estimated from x-ray studies. Moreover, parameters like microstrain, lattice stress, energy density and Young's modulus and were obtained from W-H technique according to

UDM, USDM and UDEDM. From SEM studies, it is found that The MgO NPs exhibited smooth spherical shapes with typical diameters in the range of 65±5 nm. The as-prepared MgO nanoparticles demonstrated excellent photocatalytic properties as it almost completely degraded (~97%) methylene blue dye under light illumination. Favorable formation of O_2^- radicals on the MgO(001) surface is predicted from first-principles DFT calculations as the primary drivers of the MB dye degradation. The obtained results demonstrate that MgO nanoparticles are potential candidates for photocatalytic degradation of organic dyes.

REFERENCES

1. Y. Miao, X. Xu, K. Liu, S. Yu, Y. Wang, S. Yang. Preparation and Activity Evaluation of the Novel Cu/TiO_2 Nanometer Photocatalytic Materials. Sci. Adv. Mater. 12, 1027–1033 (2020).

2. J. Shang, W. Zou, P. Wang, A. Li, M. Zhou, P. Luo. Preparation and Characterization of Hollow Zinc Oxide Nanofibers and Investigation of Its Photocatalytic Properties. J. Nanoelectron. Optoelectron. 16, 64–71 (2021)

3. B. Wang, R. Zhang, J. Xu, S. Qin, J. Zheng, Y. Bian, Y. Liu, B. Shen. Effect of Calcination Temperature on Light Absorption and Visible Light Photocatalytic Activity of N Doped TiO_2 Nano-Crystalline. Sci. Adv. Mater. 12, 449–453 (2020)

4. S. Panimalar, R. Uthrakumar, E. Tamil Selvi, P. Gomathy, C. Inmozhi, K. Kaviyarasu, J. Kennedy, Studies of MnO_2/g-C_3N_4 hetrostructure efficient of visible light photocatalyst for pollutants degradation by sol-gel technique. Surfaces and Interfaces 20 (2020) 100512.

5. KaviyarasuKasinathan, John Kennedy, ManikandanElayaperumal, Mohamed Henini, Maaza Malik. Photodegradation of organic pollutants RhB dye using UV simulated sunlight on ceria based TiO_2 nanomaterials for antibacterial applications. Scientific Reports 6 (2016) 38064.

6. X. Fuku, N. Matinise, M. Masikini, K. Kasinathan, M. Maaza, An electrochemically active green synthesized polycrystalline NiO/MgO catalyst: Use in photo-catalytic applications. Materials Research Bulletin 97 (2018) 457-465.

7. Shelja Sharma, Alex O. Ibhadon, M. GraziaFrancesconi, Surinder Kumar Mehta, SasikumarElumalai, Sushil Kumar Kansal, Ahmad Umar and S. Baskoutas, Bi_2WO_6/C-dots/TiO_2: A novel Z-scheme photocatalyst for the degradation of fluoroquinolone levofloxacin from aqueous medium, Nanomaterials 20 (2020) 910 ,1-20.

8. Meenu Saini, Brijnandan S. Dehiya and Ahmad Umar, VO_2 (M) @ CeO_2 core-shell nanospheres for thermochromic smart windows and photocatalytic applications, Ceramics International, 46 (1), (2020), 986-995.

9. RitikaAbrol, Manjot Kaur, Ahmad Umar, Surinder Kumar Mehta, Sushil Kumar Kansal, M. Ajmal Khan and H. Algarni, Enhanced solar light mediated photocatalytic degradation of brilliant green dye in aqueous phase using $BiPO_4$ nanospindles and $MoS_2/BiPO_4$ nanorods. Journal of Materials Science: Materials in Electronics 30 (2019) 20741-20750.

10. X. Ma, R. Dang, J. Liu, F. Yang, H. Li, Y. Zhang, J. Luo. Facile Synthesis and Characterization of Spinel $NiFe_2O_4$ Nanoparticles and Studies of Their Photocatalytic Activity for Oxidation of Alcohols. Sci. Adv. Mater. 12, 357–365 (2020)

11. Y.X. Wei, M. G. Ma, S. Y. Li, F. Liu, G. H. Zhao, Visible Light Activity in Phenol Degradation of $C_{60}@P_{25}$ Photocatalyst with Core–Shell Structure. J. Nanoelectron. Optoelectron. 15, 189–196 (2020)

12. MuhudJulkabli N, Bagheri S, Bee Abd Hamid S, Recent advances in heterogeneous photocatalytic decolourization of synthetic dyes, Scientific world Journal (2014)

13. K. Kaviyarasu, C. Maria Magdalane, D. Jayakumar, Y. Samson, A. K. H. Bashir, M. Maaza, Douglas Letsholathebe, Ahmed Hossam Mahmoud, J. Kenned, High performance of pyrochlore like $Sm_2Ti_2O_7$ heterojunctionphotocatalyst for efficient degradation of rhodamine-B dye with wastewater under visible light irradiation. Journal of King Saud University-Science 32 (2020) 1516-1522.

14. Ya-Jie Jing, Le Kang, Hui-Ling Du, Xian Du, Xin-Rui Jing, Long Bai, and Yao-Jun Zhang, Preparation and Photocatalytic Properties of Novel Alkali-Activated-Steel-Slag-Based Composite. Sci. Adv. Mater. 12, 1695–1701 (2020)

15. Xuan Fang, Dan Fang, Hongbin Zhao, Mukfung Yuen, Bobo Li, XiaoyuQuan, Zhikun Xu, and Zhen Guo. *In Situ* Photocurrent Spectroscopy and Photocatalysis of Heterojunctions

Based on BiOCl/MgO/ZnO Core/Shell Nanosheets. J. Nanoelectron. Optoelectron. 15, 1053–1058 (2020)

16. Liang Guo, Xuan Fang, Zhikun Xu, Yaodan Chi, Dan Fang, and Xiaotian Yang. Improving the Optical and Photocatalytic Properties of ZnO Nanowires with Atomic Layer Deposited TiO2 Shell Structures. J. Nanoelectron. Optoelectron. 15, 1023–1027 (2020)

17. Savita Chaudhary, Yesbinder Kaur, BhumikaJayee, Ganga Ram Chaudhary, Ahmad Umar, NiO nanodisks: highly efficient visible-light driven photocatalyst, potential scaffold for seed germination of VignaRadiata and antibacterial properties. Journal of Cleaner Production 190 (2018) 563-576.

18. Pankaj Taneja, Shelja Sharma, Ahmad Umar, Surinder Kumar Mehta, Alex O. Ibhadon, Sushil Kumar Kansal, Visible-light driven photocatalytic degradation of brilliant green dye based on cobalt tungstate nanoparticles. Materials Chemistry and Physics 211 (2018) 335-342.

19. Ramesh Kumar, Ahmad Umar, D.S. Rana, P. Sharma, M.S. Chauhan and S. Chauhan, Fe-doped ZnO nanoellipsoids for enhanced photocatalytic and highly sensitive and selective picric acid sensor. Materials Research Bulletin 102 (2018) 282-288.

20. Haibin Zheng and Hongxia Bu. Morphology Adjustment of TiO2 Nanostructures for Enhanced Photocatalytic Properties. J. Nanoelectron. Optoelectron. 15, 184–188 (2020)

21. K. Kaviyarasu, E. Manikandan, J. Kennedy, M. Maaza. A comparative study on the morphological features of highly ordered MgO:AgOnanocube arrays prepared *via* a hydrothermal method. RSC Advances 5 (2015) 82421-82428.

22. Y. Subba Reddy, C. Maria Magdalane, K. Kaviyarasu, Genene TessemaMola,J. Kennedy, M. Maaza.Equilibrium and kinetic studies of the adsorption of acid blue 9 and Safranin O from aqueous solutions by MgO decked FLG coated Fuller's earth. Journal of Physics and Chemistry of Solids. 123 (2018) 43-51.

23. SahandJorfi, GelavizhBarzegar, Mehdi Ahmadi,Reza DarvishiCheshmehSoltani, NematalahJafarzadehHaghighifard, AfshinTakdastan, Reza Saeedi , MehrnooshAbtahi, Enhanced coagulation-photocatalytic treatment of Acid red 73 dyeand real textile wastewater using UVA/synthesized MgO nanoparticles, Journal of Environmental Management, 177 (2016) 111-118

24. Wei Zhang, Hui LinTay, Sze ShengLim, YongshengWang, ZiyiZhong, RongXu, Supported cobalt oxide on MgO: Highly efficient catalysts for degradation of organic dyes in dilute solutions, Applied Catalysis B: Environmental 95 (2010) 93–99.

25. K. Karthik, S. Dhanuskodi, S. Prabu Kumar, C. Gobinath, S. Sivaramakrishnan, Microwave Assisted Green Synthesis of MgO Nanorods and the antibacterial and anti- breast cancer activities. 206 (2017) 217-220.

26. Mumthasharma, Dimple Gandhi and Minakshi Sharma, Synthesis of nano structured Magnesium Oxide by sol-gel method and its characterization, International Journal of Pharmaceutical Sciences and Research, 9 (2018) 1576- 1581.

27. Gottimukkala KSV, Harika Reddy P, DeevekaZamare, Green synthesis of Iron NPs using Green tea leaves extract, Nanomedicine, Biotherapeutic discovery (2017) 7:1.

28. K. Maheswari, Sawanta S. Mali, R. Sathyamoorthy, Pramod S. Patil, Template- free synthesis of MgO nanoparticles for effective photocatalytic application, Powder Technology 249(2013) 456- 462.

29. X. Ke, N. Qin, T. Zhang, F. Ke, X. Yan, Highly Augmented Antioxidant and Anticancer Effect of Biocompatible MIL-100(Fe)@SiO$_2$-Immobilized Green Tea Catechin, Journal of Inorganic and Organometallic Polymers and Materials, 30 (2020) 935–942.

30. F. Ke, M. Zhang, N. Qin, G. Zhao, J. Chu, X. Wang, Synergistic antioxidant activity and anticancer effect of green tea catechin stabilized on nanoscale cyclodextrin-based metal–organic frameworks. Journal of Materials Science. 54 (2019) 10420-10429.

31. JaisonJeevanandam, Yen San Chan and Michael K. Danquah, Biosynthesis and characterization of MgO NPs from plant extracts via induced molecular nucleation, New Journal of Chemistry 41 (2017) 2800-2814.

32. PrasantaSutradhar, MitaliSaha, DebasishMaiti, Microwave synthesis of copper oxide nanoparticles using tea leaf and coffee powder extracts and its antibacterial activity, Journal of NanostructChem 4:86 (2014) 1-6.

33. Brijesh Pare, Pardeep Singh and S B Jonnalagadda, Degradation and mineralization of methylene blue B dye in a slurry photoreactor using advanced oxidation process, Journal of Scientific & Industrial Research, 68 (2009) 724-729.

34. Mamta Yadav, S. Ali1 and O. P. Yadav, Photocatalytic degradation of Methylene Blue-B Dye using ZnS and ZnS/Fe2O3 composite nanoparticles under visible radiation, Pelagia Research Library Der ChemicaSinica, 6 (2015) 28-37.

35. G. Kresse, J. Furthmüller, J. Hafner, Theory of the crystal structures of selenium and tellurium: The effect of generalized-gradient corrections to the local-density approximation, Phys. Rev. B, 50 (1994) 13181-13185

36. P.E. Blöchl, Projector augmented-wave method, Phys. Rev. B, 50 (1994) 17953-17979.

37. S. Grimme, J. Antony, S. Ehrlich, H. Krieg, A consistent and accurate ab initio parametrization of density functional dispersion correction (DFT-D) for the 94 elements H-Pu, J. Chem. Phys., 132 (2010) 154104.

38. J.P. Perdew, K. Burke, M. Ernzerhof, Generalized gradient approximation made simple. Phys. Rev. Lett., 78 (1997) 1396-1396.

39. G.W. Watson, E.T. Kelsey, N.H. de Leeuw, D.J. Harris, S.C. Parker, Atomistic simulation of dislocations, surfaces and interfaces in MgO, J. Chem. Soc. Faraday Trans., 92 (1996) 433-438

40. W. Tang, E. Sanville, G. Henkelman, A grid-based Bader analysis algorithm without lattice bias, J. Phys. Condes. Matter, 21 (2009) 084204.

41. M. Sundrarajan, J.Suresh, R.Rajiv Gandhi, A Comparative Study on Antibacterial Properties Of MgO Nanoparticles Prepared Under Different Calcination Temperature, Journal of Nanomaterials and Biostructures 7 (2012) 983 – 989.

42. ArivazhaganPugaizhendi, Raju Prabhu, KavithaMuruganantham, RajasreeShanmuganathan, Suganthy Natarajan, Anticancer, Antimicrobial and photocatalytic activities of green synthesized MgO NPs using aqueous extract of sargassumWightti, Journal of Photochemistry & Photobiology, B: Biology 190 (2019) 86-97.

43. Kibasomba, Pierre M., Simon Dhlamini, Malik Maaza, Chuan-Pu Liu, Mohamed M. Rashad, Diaa A. Rayan, and Bonex W. Mwakikunga. Strain and grain size of TiO2 nanoparticles from TEM, Raman spectroscopy and XRD: The revisiting of the Williamson-Hall plot method. Results in Physics 9 (2018): 628-635.

44. Iwayan Sutapa, Abdul Wahid Wahab, Paulina Taba,andNursiah La Nafie, Synthesis and Structural profile analysis of the MgO NPs produced through the Sol-Gel method followed by annealing process, Oriental Journal of Chemistry 34(2) (2018) 1016-1025.

45. Neha Rani, SurjeetChahal, Anuj S. Chauhan, Parmod Kumar, Rajni Shukla, S.K. Singh, X-ray Analysis of MgO NPs by modified Scherer's Williamson-Hall and size-strain method, Materials Today: Proceedings 12 (2019) 543-548.

46. Sundaram, P. Shunmuga, T. Sangeetha, S. Rajakarthihan, R. Vijayalaksmi, A. Elangovan, and G. Arivazhagan. XRD structural studies on cobalt doped zinc oxide nanoparticles synthesized by coprecipitation method: Williamson-Hall and size-strain plot approaches. Physica B: Condensed Matter 595 (2020): 412342.

47. Zak, A. Khorsand, WH Abd Majid, M. EbrahimizadehAbrishami, and RaminYousefi. X-ray analysis of ZnO nanoparticles by Williamson–Hall and size–strain plot methods. Solid State Sciences 13, no. 1 (2011): 251-256.
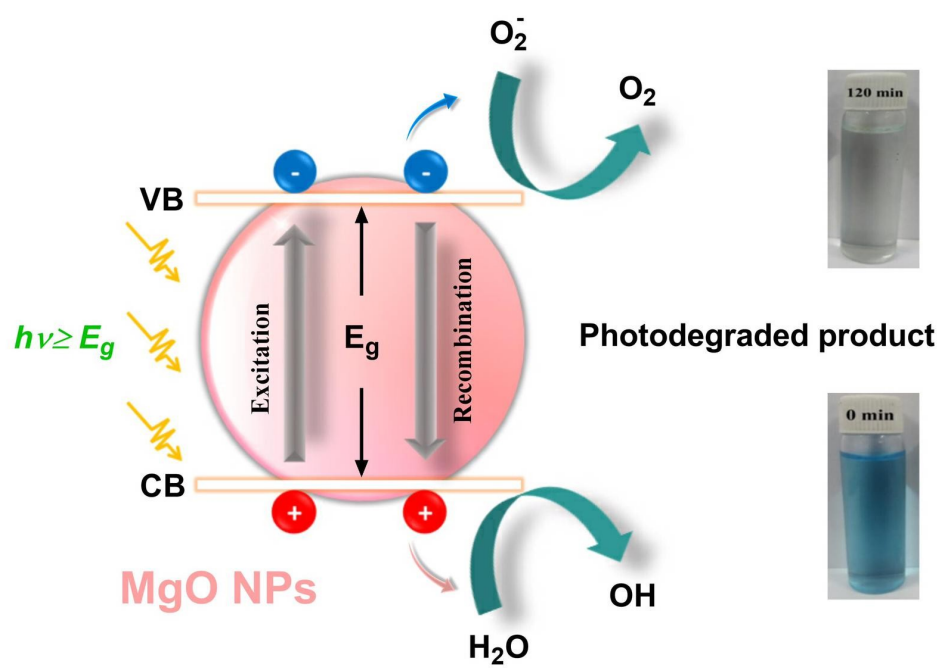
48. YendrapatiTarakaPrabhu, KalagaddaVenkateswara Rao, VemulaSesha Sai Kumar, Bandla Siva Kumari, X-ray analysis by Williamson-Hall and size-strain strain plot methods of ZnO nanoparticles with fuel variation, World Journal of Nanoscience and Engineering, 4 (2014) 21-28.

49. Yousefi, Sadegh, BehroozGhasemi, and Maria P. Nikolova. Morpho/Opto-structural Characterizations and XRD-Assisted Estimation of Crystallite Size and Strain in MgO Nanoparticles by Applying Williamson–Hall and Size–Strain Techniques. Journal of Cluster Science (2021): 1-11.

50. Rabiei M, Palevicius A, Monshi A, Nasiri S, Vilkauskas A, Janusas G. Comparing Methods for Calculating Nano Crystal Size of Natural Hydroxyapatite Using X-Ray Diffraction. *Nanomaterials (Basel)*. 2020;10(9):1627.

51. Savita, Megha Jain, Manju, AnkushVij, and Anup Thakur, Impact of annealing on the structural properties of MgO nanoparticles by XRD analysis and Rietveld refinement, AIP Conference Proceedings 2093 (2019) 020024.

52. L S Reddy Yadav, K Lingaraju, K Manjunath, G K Raghu, K H Sudheer Kumar and G Nagaraju, Synergistic effect of MgO nanoparticles for electrochemical sensing, photocatalytic-dye degradation and antibacterial activity, Materials Research Express 4 (2017) 11pages.

53. Himani Bhoi, Pragya Joshi, KhushbooPunia, Ganesh Lal, and Sudhish Kumar, Synthesis and rietveld refinement of MgO nanoparticles, AIP Conference Proceedings 2220 (2020) 2400-2406.

54. Angeles G. De la Torre, Francisco Jose Valle, Antonio H. De Aza, Direct mineralogical composition of a MgO-C refractory material obtained by Rietveld methodology, Journal of the European Ceramic Society 26 (2006) 2587–2592.

55. Dr.Ziad T. Khodair, Ahmed H.Abed, SamerG.Majeed, Synthesis and structural characterization of MgO nanoparticles, International Journal of Advanced Research in Science, Engineering and Technology, 3 (2016) 43-46.

56. Anantharaman, T. R., and J. W. Christian. The measurement of x-ray line breadths. British Journal of Applied Physics 4, no. 5 (1953): 155.

57. JaisonJeevanandam, Yen San Chan, and Michael K. Danquah, Calcination-Dependent Morphology Transformation of Sol-Gel- Synthesized MgO Nanoparticles, Materials Science inc. Nanomaterials & Polymers, 2017, 2, 10393 – 10404.

58. Essien, Enobong R., Violette N. Atasie, Taiye O. Oyebanji, and Davies O. Nwude. "Biomimetic synthesis of magnesium oxide nanoparticles using Chromolaenaodorata (L.) leaf extract." Chemical Papers (2020): 1-9.

59. Hanna, A. A., Abdelmoaty, A. S., &Sherief, M. A. (2019). Synthesis, Characterization, and Thermal Behavior of Nanoparticles of Mg (OH) 2 to Be Used as Flame Retardants. Journal of Chemistry, 2019.

60. Rahman Q. I., Ahmad M., Misra S. K., and Lohani M. (2014), "Hexagonal ZnO Nanorods Assembled Flowers for Photocatalytic Dye Degradation: Growth, Structural and Optical Properties" Superlattices and Microstructures, Vol. 64, p.p. 495-506.

61. Rahman Q. I., Lee W. J., Lee H. C, L., and Yang O. B., (2010), "Photocatalytic Degradation of Methylene Blue under visible light Cr doped Strontium Titanate (SrTiO$_3$) Nanoparticles" Journal of Nanoscience and Nanotechnology, Vol. 10, p.p. 3430-3434.

62. Rahman Q.I., Haman S., Ali A., Mehta S.K., Raja M.A., Ahmad N., Khan A.R., and Muddassir M., (2020) "Synthesis and characterizations of nitrogen (N) doped strontium titanate (SrTiO$_3$) nanoparticles for enhanced visible light driven photocatalytic degradation", Journal of Nanoscience and Nanotechnology, Vol. 20, pp., 6475–6481.

63. Rahman Q. I., Ahmad M., and Mehta S.K., (2017), 'Hydrothermal synthesis of Cr-doped SrTiO$_3$ nanoparticles for rhodamine-B dye degradation under visible light illumination", Collides and Polymer Science Vol. 295, Issue 5, p.p. 933–937.

64. Rahman Q. I., Ahmad M., Misra S. K., and Lohani M., (2013), 'Effective photocatalyticdegradation of rhodamine B by ZnO nanoparticles,' Materials Letters, vol.91, p.p.170-174.

65. N. Kitchamsetti; M. S Ramteke; S. R. Rondiya, S. R. Mulani; M. S. Patil, R. W. Cross, N. Y. Dzade; R. Devan. Experimental and DFT correlations on the photocatalytic activities of NiO nanobelts for removal of organic pollutants. Journal of Alloys and Compounds, 855 (2021) 157337.

HIGHLIGHTS

- Facile Synthesis of MgO nanoparticles using *Camellia sinensis* (tea leaves) extract as a reducing agent.
- Almost complete photocatalytic degradation of methylene blue dye using MgO nanoparticles.
- Confirmation for the favourable formation of O_2^- radicals on the MgO (001) surface by first-principles DFT calculations.

Graphical Abstract

AUTHORSHIP STATEMENT

Manuscript title: **Facile Green Synthesis of Magnesium Oxide Nanoparticles using Tea (*Camellia Sinensis*) Extract for Efficient Photocatalytic Degradation of Methylene Blue Dye**

All persons who meet authorship criteria are listed as authors, and all authors certify that they have participated sufficiently in the work to take public responsibility for the content, including participation in the concept, design, analysis, writing, or revision of the manuscript. Furthermore, each author certifies that
his material or similar material has not been and will not be submitted to or published in any other publication before its appearance

Authorship contributions

Category 1

Conception and design of study: **S. Ashok Kumar, M. Jarvin, S. S. R. Inbanathan.**

acquisition of data: **Nelson Y. Dzade**

analysis and/or interpretation of data: **Nelson Y. Dzade**

Category 2

Drafting the manuscript: **Ahmad Umar**

revising the manuscript critically for important intellectual content: **N. P. Lalla** , **Hassan Algadi, Qazi Inamur Rahman, Sotirios Baskoutas**

Category 3

Approval of the version of the manuscript to be published (the names of all authors must be listed):

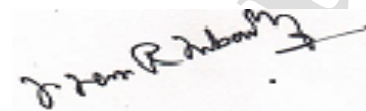**S. Ashok Kumar,**

M. Jarvin,

S. S. R. Inbanathan,

Ahmad Umar,

N. P. Lalla,

Nelson Y. Dzade,

Hassan Algadi,

Qazi Inamur Rahman,

Sotirios Baskoutas

Dr. S.S.R. INBANATHAN
Post Graduate & Research Dept. of Physics
The American College,
Madurai - 625 002.

Declaration of interests

☒ The authors declare that they have no known competing financial interests or personal relationships that could have appeared to influence the work reported in this paper.

☐ The authors declare the following financial interests/personal relationships which may be considered as potential competing interests:

S. S. R. Inbanathan